

CERN-TH/98-255
ETH-TH/98-21
hep-ph/9808262

NEXT-TO-LEADING ORDER JET CROSS SECTIONS IN POLARIZED HADRONIC COLLISIONS

Daniel de Florian

CERN, TH Division, Geneva, Switzerland

Stefano Frixione¹

Theoretical Physics, ETH, Zurich, Switzerland

Adrian Signer and Werner Vogelsang

CERN, TH Division, Geneva, Switzerland

Abstract

We present a next-to-leading order computation in QCD of one-jet and two-jet cross sections in polarized hadronic collisions. Our results are obtained in the framework of a general formalism that deals with soft and collinear singularities using the subtraction method. We construct a Monte Carlo program that generates events at the partonic level. We use this code to give phenomenological predictions for pp collisions at $\sqrt{S} = 500$ GeV, relevant for the spin physics program at RHIC. The possibility of using jet data to constrain the poorly known polarized parton densities is examined.

¹Work supported by the Swiss National Foundation.

1 Introduction

In the last few years, measurements [1] of the spin asymmetries A_1^N in deep-inelastic scattering (DIS) of longitudinally polarized lepton beams off polarized hadron ($N = p, n, d$) targets have provided much new information on the spin structure of the nucleon. Theoretical leading order (LO) [2–6] and next-to-leading order (NLO) [2–7] analyses of the data sets demonstrate, however, that these are not sufficient to accurately extract the spin-dependent quark ($\Delta q = q^\uparrow - q^\downarrow$) and gluon ($\Delta g = g^\uparrow - g^\downarrow$) densities of the nucleon. This is true in particular for $\Delta g(x, Q^2)$, since this quantity contributes to DIS in LO only via the Q^2 -dependence of A_1^N , which could not be accurately studied experimentally so far. As a result of this, it turns out [2–6] that the x -shape of Δg seems to be hardly constrained at all by the DIS data, even though a tendency towards a fairly large positive *total* gluon polarization, $\int_0^1 \Delta g(x, Q^2 = 4 \text{ GeV}^2) dx \gtrsim 1$, was found [2, 3, 4, 7]. The measurement of Δg thus remains one of the most interesting challenges for future high-energy experiments with polarized nucleons. In selecting suitable processes for a determination of Δg , it is crucial to pick those that, unlike DIS, have a direct gluonic contribution already at the lowest order. Here, one thinks in the first place of high- p_T reactions in nucleon–nucleon collisions, which have been tremendously important in the unpolarized case to constrain the unpolarized gluon density.

At the moment, the most eagerly awaited experimental tool for the ‘spin physics’ community is the RHIC collider at BNL, at which first runs in a proton–proton mode with polarized beams are expected to be accomplished in about two years from now. The centre-of-mass energy for these pp collisions will be ranging between 100 and 500 GeV, with luminosities (rising with energy) between 240 and 800 pb^{-1} , respectively. One expects about 70% polarization for each beam. Such conditions look extremely favourable for studying the spin asymmetries for all kinds of high- p_T pp processes that are sensitive to the gluon density, such as jet, prompt-photon, or heavy-flavour production. Considering the higher end of RHIC energies, jets could be *the* key to Δg : at $\sqrt{S} = 500$ GeV, clearly structured jets will be extremely copiously produced, and jet-observables will show a strong sensitivity to Δg thanks to the dominance [8] of the gg and qg initiated subprocesses in some kinematical ranges.

In order to make reliable quantitative predictions for a high-energy process, it is crucial to determine the NLO QCD corrections to the Born approximation. Quite in general, the key issue here is to check the perturbative stability of the process considered, i.e. to examine the extent to which the NLO corrections affect the cross sections and (in spin physics) the spin asymmetries relevant for experimental measurements. Only if the corrections are under control can a process that shows good sensitivity to, say, Δg at the lowest order be regarded as a genuine probe of the polarized gluon distribution and be reliably used to extract it from future data.

NLO QCD corrections are expected to be particularly important for the case of jet-production, since it is only at NLO that the QCD structure of the jet starts to play a rôle in the theoretical description, providing for the first time the possibility to realistically match the experimental conditions imposed to define a jet.

The calculation of the NLO QCD corrections to jet production by polarized hadrons is the purpose of this paper. Such a calculation needs the one-loop $2 \rightarrow 2$ and tree-level $2 \rightarrow 3$ polarized (i.e. *not* summed over external helicities) amplitudes as input. Fortunately,

these amplitudes are already known [9, 10]. Furthermore, several independent methods to calculate any infrared-safe quantity in any kind of hard unpolarized collision are at present available in the literature [11, 12, 13]. The formalism of ref. [12] has been used in ref. [14] to construct a Monte Carlo code that can calculate any three-parton infrared-safe observable in hadron–hadron unpolarized collisions. In the present paper, we will extend the method of refs. [12, 14] and adapt the Monte Carlo code to the case of polarized hadron–hadron collisions. As a result, we will present a customized code, with which it will be possible to calculate any infrared-safe quantity corresponding to either single- or di-jet production to NLO accuracy.

The outline of the paper is as follows: In section 2 we describe the calculation of next-to-leading order corrections to jet cross sections in polarized hadronic collisions. Since there is no conceptual difference to the unpolarized case, we restrain from repeating all details and only give an overview. A crucial input for the next-to-leading order calculation is the polarized gluon distribution function. Section 3 summarizes the current situation and discusses the main assumptions that are used to constrain the various fits. We begin our phenomenological study in section 4, with the investigation of the perturbative stability and reliability of our next-to-leading order results for single-inclusive as well as double-differential observables. In section 5 we turn to the more phenomenological issue of the dependence of the cross sections on the various parametrizations of the parton densities. In particular, we will also investigate some spin asymmetries. Finally, in section 6 we present our conclusions. Some technical details concerning the difference between the calculations of the cross section in polarized and unpolarized hadronic collisions are given in an appendix.

2 Formalism

We start by writing a generic differential jet cross section in polarized hadronic collisions using the factorization theorem [15]

$$d\sigma^{(H_1 H_2)}(K_1, \Lambda_1; K_2, \Lambda_2; \mathcal{S}) = \sum_{a_1 a_2} \sum_{\lambda_1 \lambda_2} \int dx_1 dx_2 f_{a_1 \lambda_1}^{(H_1 \Lambda_1)}(x_1) f_{a_2 \lambda_2}^{(H_2 \Lambda_2)}(x_2) \times d\hat{\sigma}_{a_1 a_2}(x_1 K_1, \lambda_1; x_2 K_2, \lambda_2; \mathcal{S}), \quad (2.1)$$

where H_1 and H_2 are the incoming hadrons, with momenta K_1 and K_2 and helicities Λ_1 and Λ_2 respectively; $f_{a_i \lambda_i}^{(H_i \Lambda_i)}$ is the non-calculable but universal distribution function for the parton a_i with helicity λ_i in the hadron H_i with helicity Λ_i and $d\hat{\sigma}_{a_1 a_2}$ are the (subtracted) short-distance partonic cross sections². The quantity \mathcal{S} is the measurement function; it defines the jet momenta in terms of the parton momenta. Its specific form therefore depends upon the jet-clustering algorithm adopted. Since the results for polarized scattering are

²In the following, we will often omit some of the entries of the quantity $d\hat{\sigma}_{a_1 a_2}$; the meaning should be clear from the context.

usually presented in terms of the quantity

$$d\Delta\sigma^{(H_1H_2)} = \frac{1}{4} \left(d\sigma^{(H_1H_2)}(+;+) + d\sigma^{(H_1H_2)}(-;-) \right. \\ \left. - d\sigma^{(H_1H_2)}(+;-) - d\sigma^{(H_1H_2)}(-;+) \right), \quad (2.2)$$

it is convenient to rewrite eq. (2.1) in the following form:

$$d\Delta\sigma^{(H_1H_2)}(K_1; K_2; \mathcal{S}) = \sum_{a_1 a_2} \int dx_1 dx_2 \Delta f_{a_1}^{(H_1)}(x_1) \Delta f_{a_2}^{(H_2)}(x_2) d\Delta\hat{\sigma}_{a_1 a_2}(x_1 K_1; x_2 K_2; \mathcal{S}), \quad (2.3)$$

where $d\Delta\hat{\sigma}_{a_1 a_2}$ is defined analogously to $d\Delta\sigma^{(H_1H_2)}$ in eq. (2.2), and

$$\Delta f_{a_i}^{(H_i)} = f_{a_i+}^{(H_i+)} - f_{a_i-}^{(H_i+)} = f_{a_i-}^{(H_i-)} - f_{a_i+}^{(H_i-)}. \quad (2.4)$$

The available parametrizations for polarized parton densities are presented in terms of the quantities $\Delta f_a^{(H)}$.

Our aim in the present paper is to evaluate the polarized cross section in eq. (2.3) at next-to-leading order in perturbative QCD, for one- and two-jet production. As is well known, there are two main problems in such a computation. First of all, the relevant polarized amplitudes have to be known. For our case, we need the $2 \rightarrow 2$ one-loop and $2 \rightarrow 3$ tree-level amplitudes. These amplitudes have been computed [9, 10] using the technique of colour ordering and the helicity method. Secondly, the cancellation of the infrared poles, which appear in the intermediate steps of the calculation, has to be performed analytically. Due to the universal (i.e. process-independent) structure of these poles, general methods [11, 12, 13] exist, which allow the computation of any infrared-safe cross section in any type of hard scattering. In the present paper we will use the approach of ref. [12], based upon the subtraction method. The main idea of ref. [12] is to exploit the properties of the measurement function in order to disentangle the infrared-singular regions that appear in the real contribution. Indeed, as follows from the universal properties of the measurement function (which are responsible for the good definition of any infrared-safe cross section), this quantity can be written as a sum of terms, each of which is non-vanishing only when one given parton is soft or collinear to another parton. Therefore, the partonic cross section can be expressed as a sum of terms whose singular structure is trivial, and the subtraction procedure can be straightforwardly implemented. It is important to notice that, although the approach of ref. [12] was originally introduced in the case of unpolarized collisions, it does not need any principle modification to be applied to the case of polarized collisions, since the major rôle in the treatment of the singularities is played by the measurement function. Further details on this topic can be found in the appendix.

The procedure of ref. [12] results in the subtracted partonic cross sections which appear in eqs. (2.1) or (2.3). Standard Monte Carlo methods can therefore be used to compute the quantity

$$\langle H \rangle = \int d\Delta\sigma^{(H_1H_2)}(\mathcal{S}) H, \quad (2.5)$$

where H is any function of the jet momenta, which are defined by \mathcal{S} . If H is a product of θ functions, implementing experimental cuts and selecting a bin of a given histogram, then $\langle H \rangle$ is the QCD prediction for the cross section in that bin.

The main drawback of eq. (2.5) is that the jet definition is used, through the measurement function, to disentangle the infrared singularities. This prevents us from getting predictions for different jet definitions when performing a single computer run, as is customary in a parton shower Monte Carlo; also, one-jet and two-jet observables must be treated separately. This problem was addressed in ref. [14]; the key observation is that, in order to disentangle the infrared singularities, the measurement function can be substituted by a suitable sum of products of θ functions, which we call the \mathcal{P} function. By construction, each term of the sum is non-vanishing only in one given infrared-singular region which contributes to the cross section at next-to-leading order. In this sense, the \mathcal{P} function and the \mathcal{S} function are completely equivalent, and the former can be interpreted as a fake measurement function (however, while the real measurement function contains δ functions that define the jet momenta in terms of the parton momenta, the \mathcal{P} function only contains θ functions). Therefore, following ref. [14], we can write the analogue of eq. (2.5) as

$$[H\mathcal{S}] = \int d\Delta\sigma^{(H_1 H_2)}(\mathcal{P}) H \mathcal{S}. \quad (2.6)$$

By construction, we get $\langle H \rangle = [H\mathcal{S}]$. A computer program based upon eq. (2.5) outputs jet momenta, which are eventually used to fill a histogram as specified by H . On the other hand, a computer program based upon eq. (2.6) outputs parton momenta; these quantities are eventually used to compute jet momenta (as specified by \mathcal{S}), which will again fill the histogram given by H . Therefore, in eq. (2.6) no jet definition is involved in the generation of the hard event and in the computation of the weight. It follows that, during the same computer run, it is possible to use several different jet definitions and to compute one-jet, two-jet and non-jet (like transverse thrust) observables. This kind of computer code is called a *parton generator*.

In ref. [14] two parton generators were presented, one for photon-hadron collisions and one for hadron-hadron collisions. The latter has been suitably modified to deal with polarized hadron-hadron collisions, and used to produce the phenomenological results presented in this paper. The structure of the code of ref. [14] remains unchanged, since only the unpolarized partonic cross sections and splitting functions had to be substituted with the polarized ones (see the appendix for more details).

3 Polarized Parton Distribution Functions

As stated in the introduction, there is hardly any experimental information on the spin-dependent gluon density Δg at present. In contrast, the quark densities are far better constrained by the existing data from inclusive polarized DIS. This is particularly true for the polarized valence quark densities, which come out rather similar in all theoretical analyses performed so far. The spin-dependent sea-quark distributions seem less well constrained;

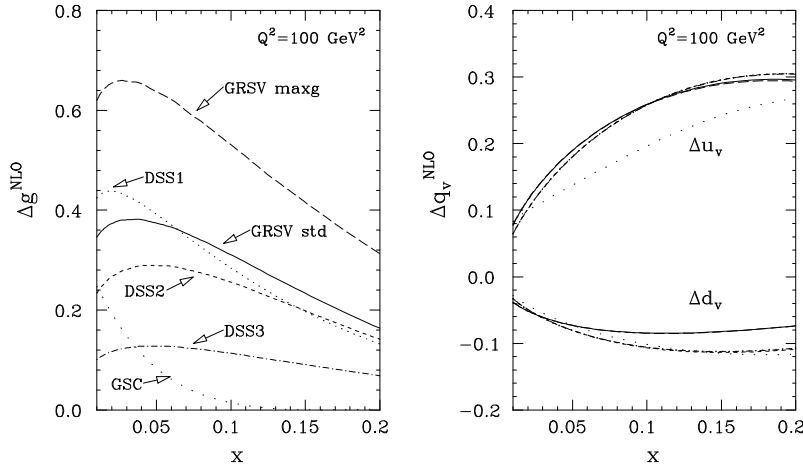


Figure 1: The polarized gluon (left) and valence quark densities (right), as given by the six NLO parametrizations that will be used in this paper, at the scale $Q^2 = 100 \text{ GeV}^2$. The patterns for the quark densities are the same as those used for the gluon.

however, they are of minor importance for our jet studies³.

In our phenomenological analysis we will try to cover as much as possible of the wide range of polarized parton densities allowed by the present DIS data: this is especially relevant for the gluon density, as we will discuss below. We will use the following six polarized parton density sets, which were obtained within various theoretical analyses of polarized DIS:

- Two sets of ref. [2], the ‘standard’ set, corresponding to the best fit to the data obtained in ref. [2] (from now on, referred to as GRSV std), and a set obtained when saturating the positivity constraint $|\Delta g| \leq g$ for the gluon density at the low input scale $\mathcal{O}(0.5 \text{ GeV})$ (GRSV maxg).
- The three sets of ref. [4] (DSS1, DSS2, DSS3), obtained by constraining the first moment of the polarized gluon densities in three different ways. The first moment of the gluon of DSS1 is the largest and almost one order of magnitude larger than for DSS3, which has the smallest gluon.
- Set C of ref. [3] (GS-C), which provides a gluon distribution with a qualitatively different x -shape, becoming negative at large x for low Q^2 . Sets A and B of ref. [3] are similar to some of the GRSV and DSS ones, and we do not use them so as to avoid a proliferation of curves.

³Strictly speaking, inclusive DIS data for proton and neutron targets can only give information on the two non-singlet and the quark singlet combinations, rather than on all quark and antiquark densities individually. The inclusion of data [1] for the spin asymmetry in semi-inclusive DIS (SIDIS), which in principle would allow a complete flavour discrimination in the quark sector, does not provide much help in practice, since the SIDIS data have not yet reached the precision of the inclusive ones. The flavour decomposition of the nucleon parton densities – which is essential for making predictions for observables other than DIS – therefore partly depends on theoretical assumptions made when analysing the DIS data [2–5].

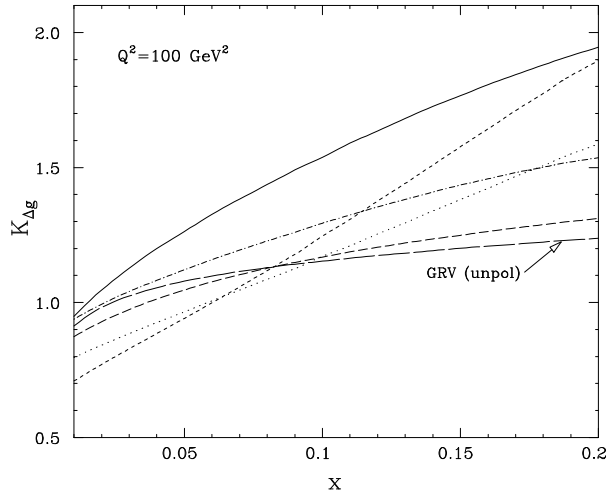


Figure 2: *Ratio of NLO to LO polarized gluon densities. We use the same pattern as in fig. 1 to distinguish the various lines. Also shown is the ratio for an unpolarized (GRV) set.*

All these distributions are available at both LO and NLO, the latter corresponding to the $\overline{\text{MS}}$ scheme used also in our calculation of the NLO partonic cross section.

In this work, we will analyse the phenomenology of polarized jet production for the particular case of RHIC at a centre-of-mass energy of $\sqrt{S} = 500$ GeV and for jet transverse momenta in the region of $15 \text{ GeV} < p_T < 100 \text{ GeV}$. This implies that the polarized parton distributions will mainly be probed in the x -range $0.06 \lesssim x \lesssim 0.4$ and at typical scales Q^2 of the order of 100 GeV^2 . Figure 1 shows the NLO polarized valence quark and gluon densities of the six different sets we are going to use. It becomes obvious that there is indeed a wide range of possible gluon distributions compatible with present polarized DIS data. As mentioned earlier, in the valence sector, most of the distributions are very similar, with slight exceptions in the cases of the u_v distribution of GS-C and the d_v density of GRSV std. The origin of these differences can be easily traced back to the fact that the analyses of refs. [2, 3] are based on a somewhat smaller data sample than the others, since some data sets became available only after [2, 3] had been published. The spin-dependent sea-quark densities (not shown in fig. 1) differ more strongly among the various sets, but have only a very small impact on the jet cross sections in this kinematical region: they only amount to less than 5% of the contribution from valence quarks. In conclusion, since the variations in the quark sector are much smaller than the ones for gluons, we can expect that any differences between predictions for the polarized jet cross sections (or asymmetries) that are found when using different polarized parton density sets, are to be attributed to the sensitivity of the observable to Δg .

The size of radiative QCD corrections to a given unpolarized hadronic process is often displayed in terms of a ‘ K -factor’ which represents the ratio of the NLO over LO results. In the calculation of the numerator of K one obviously has to use NLO-evolved parton densities. As far as the denominator is concerned, a natural definition requires the use

of LO-evolved parton densities. However, by using NLO-evolved parton densities and LO partonic cross sections, one still obtains a hadronic cross section accurate to LO, and therefore the denominator of the K -factor can also be computed with NLO-evolved parton densities. If one chooses a ‘natural’ subtraction scheme, such as $\overline{\text{MS}}$, these two definitions of the K -factor are expected to give similar results (we stress that the two definitions might give rather different results in the framework of an arbitrary subtraction scheme: there is no reason to worry about that, since the K -factor is *not* a physical quantity, and therefore it is not supposed to be scheme-independent). However, in the case of polarized scattering, additional problems arise. Indeed, suppose one attempts to fit Δg from the DIS data. Since the data hardly constrain the gluon density, very different results for Δg can emerge if the fit is performed at LO or at NLO. This is confirmed in fig. 2, where we show the ‘gluonic’ K -factors $K_{\Delta g} \equiv \Delta g^{\text{NLO}}/\Delta g^{\text{LO}}$ as functions of x for our various sets⁴. It can be seen that indeed for most sets $K_{\Delta g}$ is *not* close to unity. We observe that things are much better in the unpolarized case, where there are far more data to constrain the gluon: here $K_g \equiv g^{\text{NLO}}/g^{\text{LO}} \approx 1$. Also note that in the case of the ‘GRSV maxg’ set, where one assumes [2] that $\Delta g^{\text{LO,NLO}} = g^{\text{LO,NLO}}$ at the input scale (see above) in both LO and NLO, a $K_{\Delta g} \approx 1$ is found also at higher scales. This underlines our point that artificially large or small K -factors for, say, polarized jet production could result merely from the fact that the gluon is at present so ill-constrained. We will discuss this point further in section 4.

4 Perturbative Stability

As we mentioned in the previous section, in the case of polarized collisions the study of the K -factor, which in general does not give any information on the perturbative stability of the results in hadronic scattering, faces additional problems, due to the large difference between Δg^{NLO} and Δg^{LO} . To illustrate this issue, we have computed the LO hadronic cross section entering the K -factor in two different ways, by convoluting the partonic LO cross sections with either LO-evolved parton densities or NLO-evolved parton densities. For the sole purpose of distinguishing the two definitions, we will call the former the tree-level cross section and the latter the Born cross section. As an example we have chosen the p_T spectrum, using the Ellis–Soper (ES) cluster jet algorithm as proposed in ref. [16] with the resolution parameter $D = 1$. In fig. 3a we show the ratio of the NLO cross section over the tree-level cross section. This ratio can be rather large for some parton density sets. However, a comparison with fig. 2 shows that these large corrections come mainly from the change of Δg^{LO} to Δg^{NLO} . Indeed, if we plot the ratio of the NLO cross section over the Born cross section, as done in fig. 3b, we see that the corrections are moderate. For the same reason as in fig. 2 we do not show the curve for the GS-C set. On the other hand, we also show the same ratio for the unpolarized case, using the GRV parton densities [17].

A reliable error estimate on our NLO results requires some knowledge on the size of the uncalculated higher-order terms. The only fully reliable way to get this information is to perform computations of even higher order. Unfortunately, such a calculation is currently out of reach. Thus, the best we can do is to study the dependence of the full NLO results on

⁴We do not show $K_{\Delta g}$ for GS-C, since in this case Δg^{LO} may be zero.

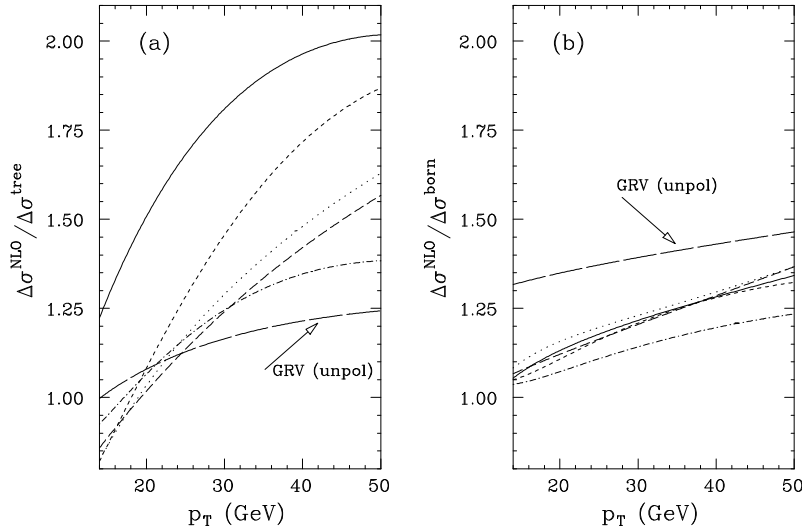


Figure 3: *Ratio of the next-to-leading order cross section over (a) the tree-level cross section (i.e. leading order pdf) and (b) the Born cross section (i.e. next-to-leading order pdf) for various parton densities. We use the same pattern as in fig. 1 to distinguish the various parton densities.*

the renormalization and factorization scales. Throughout we will set the two scales equal, i.e. $\mu_R = \mu_F \equiv \mu$. Although physical observables are obviously independent of μ , theoretical predictions do have such a dependence. It arises from the truncation of the perturbative expansion at a fixed order in the strong coupling constant α_s . A large dependence on μ , therefore, implies a large theoretical uncertainty.

The scale dependence of the tree-level and Born cross section is very similar. For the rest of this paper we will always use the Born cross section (i.e. the leading order hard partonic cross section integrated over the next-to-leading order parton densities) as the leading order result. As we will see, the scale dependence is substantially reduced once the next-to-leading order corrections are included.

We will always consider proton-proton scattering with $\sqrt{S} = 500$ GeV. For the strong coupling constant α_s we use the standard two-loop form with Λ_{QCD} set to the value used in the parton distribution function under consideration. Our default choice for the scale is

$$\mu_0 \equiv \frac{1}{2} \sum_i k_{iT}, \quad (4.1)$$

where the sum is over all final-state partons and k_{iT} is the transverse momentum of parton i . We will study the scale dependence of several observables by comparing the results obtained with $\mu = \mu_0$ with those obtained with $\mu = \mu_0/2$ and $\mu = 2\mu_0$, in both the polarized and unpolarized cases. For this purpose, we fix the parton distribution functions: our default choices are MRST [18] and GRSV std [2] for the unpolarized and the polarized case respectively. We verified that our conclusions are unchanged when using other density sets.

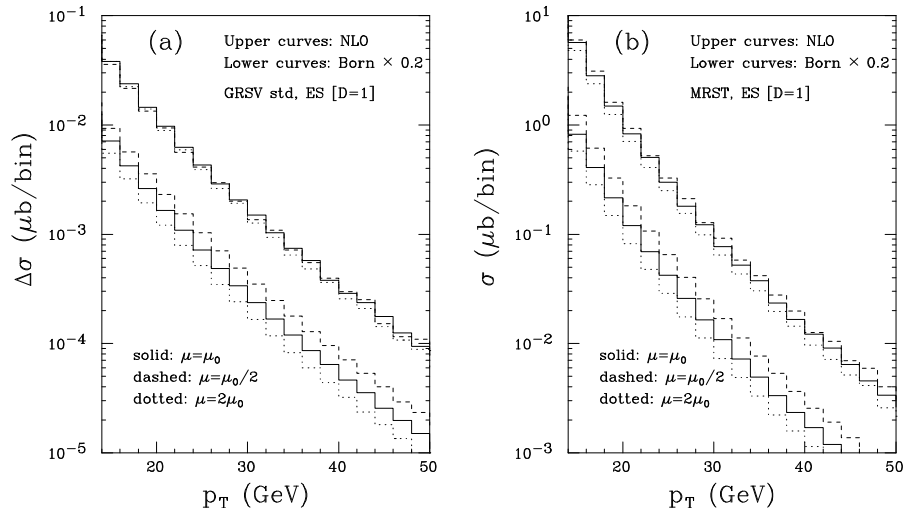


Figure 4: Scale dependence of the next-to-leading order and Born p_T -distributions for the Ellis-Soper algorithm with $D = 1$. (a) Polarized pp scattering and (b) unpolarized pp scattering at $\sqrt{S} = 500$ GeV. The range of the pseudo-rapidity is restricted to $|\eta| < 1$.

To start with, we consider the inclusive p_T -distributions, where p_T is the transverse momentum of the jet. As in fig. 3, we use the cluster jet algorithm with the resolution parameter $D = 1$ and require $|\eta| < 1$. We checked that, basically, the definition of a jet through a cone algorithm only amounts to a change in the normalization. Concerning the scale dependence, the different jet definitions give very similar results. In fig. 4a we show the next-to-leading and leading order distributions in the polarized case for the three different scales: μ_0 , $2\mu_0$ and $\frac{1}{2}\mu_0$. Note that the Born results have been rescaled in order to disentangle the two sets of curves. Figure 4b is the corresponding plot for the unpolarized case. Clearly, the dependence on the scale is substantially reduced when going to next-to-leading order. The situation in the polarized case is indeed very similar to the unpolarized one.

We also investigated the distribution in pseudo-rapidity and verified that the scale dependence is reduced in a similar manner as for the p_T -distribution. Again, the dependence on the scale is very similar to the unpolarized case.

A more stringent test on the perturbative stability of fixed-order QCD calculations can be made by considering quantities that are more exclusive than single-inclusive ones. At next-to-leading order, this basically means double-differential cross sections. Although the definition of these quantities is to some extent arbitrary, we will use the most commonly adopted prescription: we select all the events with two or more jets, we apply suitable cuts to the two leading jets (i.e. those with the largest transverse momentum) of each event, and we finally compute correlations between these two leading jets. To be specific, we require

$$p_{1T} > p_{1T}^{cut}, \quad |\eta_1| < 1, \quad p_{2T} > p_{2T}^{cut}, \quad |\eta_2| < 1, \quad (4.2)$$

where p_{iT} and η_i denote the transverse momenta and the pseudo-rapidities of the two leading

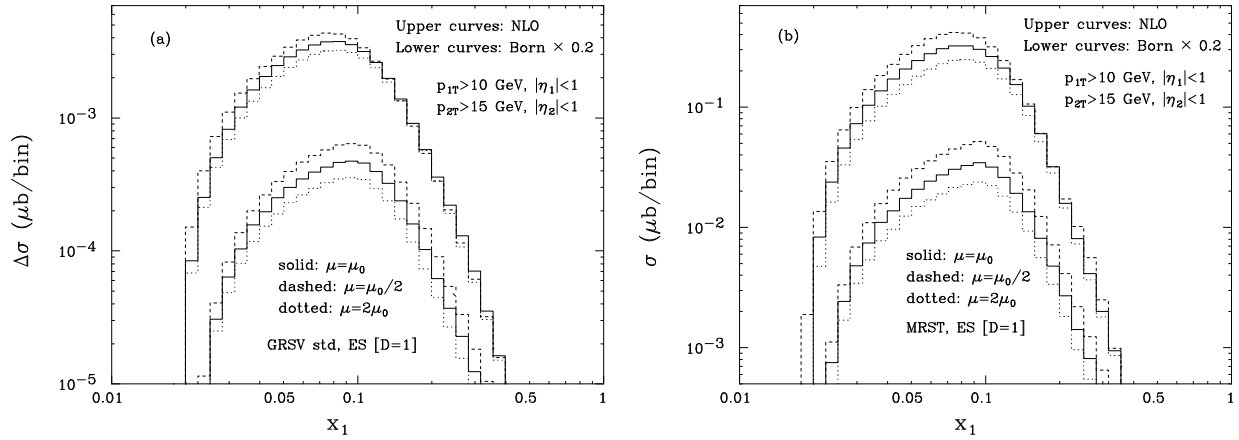


Figure 5: As in fig. 4, for the x_1 -distribution (see the text for the definition).

jets. We considered the two cases

$$p_{1T}^{cut} = p_{2T}^{cut} = 10 \text{ GeV}, \quad (4.3)$$

and

$$p_{1T}^{cut} = 10 \text{ GeV}, \quad p_{2T}^{cut} = 15 \text{ GeV}, \quad (4.4)$$

and studied various correlations, such as the angular distance in the plane perpendicular to the beam axis $\Delta\phi_{jj}$, the invariant mass M_{jj} and the transverse momentum p_T^{jj} of the pair, the difference in pseudo-rapidity of the two jets $\Delta\eta_{jj}$ and so on. In the case when the cuts given in eq. (4.4) are applied, we find that the next-to-leading order results are more stable (with respect to scale variations) than the corresponding Born ones, where this comparison makes sense (there are regions of the phase space that are not accessible at the Born level. A typical example, with the cuts of eq. (4.4), is the threshold in the invariant mass distribution. In these regions, the NLO results display a scale dependence that is larger than anywhere else. This is what we expect, since in these regions our results are effectively leading order results). As an example, we present in fig. 5 the distribution in the variable x_1 , defined as follows

$$x_1 = \frac{p_{1T} e^{\eta_1} + p_{2T} e^{\eta_2}}{\sqrt{S}}. \quad (4.5)$$

The variable x_1 roughly corresponds to the momentum fraction of one of the two partons of the scattering process, and it is exactly so at the Born level. From the figure, we see that the NLO result has an enhanced scale dependence in the region of small x_1 ; this is due to the fact that the small x_1 values correspond to almost back-to-back jets, that is to a configuration which is sensitive to soft gluon emission. However, in the whole remaining range of x_1 the scale dependence of the NLO result is smaller than that of the Born result.

The case when the cuts given in eq. (4.3) are applied is more problematic in the framework of a fixed-order QCD calculation. This situation has been discussed in great detail in ref. [19]; here, we just remind the reader that, although the cuts given in eq. (4.3) define

an infrared-safe cross section (and can therefore be implemented without any problem by the experiments), there are regions in the phase space (basically, all those corresponding to an exactly back-to-back configuration of the two leading jets) where any fixed-order QCD calculation breaks down, and an all-order resummation would be required. We explicitly verified that, in the regions $\Delta\phi_{jj} \simeq \pi$, $p_T^{jj} \simeq 0$ and close to the threshold in M_{jj} , the scale dependence of the NLO result is much larger than that of the LO result, thus signalling a failure in the perturbative expansion. However, we stress that, in all the remaining regions of the phase space, the cuts of eq. (4.3) result in a cross section as well behaved as that obtained by applying the cuts of eq. (4.4).

Finally we would like to mention that we have computed all the aforementioned distributions by using both the ES and the cone jet-finding algorithms. We observed only minor differences between the two resulting cross sections.

5 Dependence of Observables upon Parton Densities

Up to this point, we have shown that the polarized jet cross sections at next-to-leading order display a remarkable stability under scale changes in the upper end of the energy range probed at RHIC. It is therefore sensible to use our code to investigate in some detail a few phenomenological issues relevant to hadronic physics at RHIC.

We thus turn to the problem of studying the dependence of the theoretical predictions upon the perturbatively non-calculable quantities that enter eq. (2.1), namely the parton densities and the value of Λ_{QCD} . We will not perform an analysis of the separate dependence of our results upon these two quantities, since the polarized parton density parametrizations are only available with a single value of Λ_{QCD} . In the following, Λ_{QCD} will therefore always be set equal to the value associated to the various parton density sets used. In this section, our predictions are obtained by defining the jets with the ES algorithm with $D = 1$, and the scales have been set to the default value $\mu = \mu_0$.

We start by considering the asymmetry

$$\mathcal{A}_{p_T} = \frac{d\Delta\sigma/dp_T}{d\sigma/dp_T}. \quad (5.1)$$

Here $\Delta\sigma$ and σ are the one-jet inclusive cross sections for polarized and unpolarized scattering respectively, and p_T is the transverse momentum of the observed jet. A cut $|\eta| < 1$ has also been applied. In fig. 6, \mathcal{A}_{p_T} is shown as a function of p_T . The results for $\Delta\sigma$ have been obtained by choosing the six different parametrizations of the polarized parton densities previously mentioned. The unpolarized cross section σ has been evaluated using the MRST set. Figure 6 clearly shows that the choice of the polarized parton densities induces an uncertainty on the theoretical results of more than two orders of magnitude. This enormous spread is basically due to the fact that the polarized gluon density is very poorly constrained by present DIS data, and at this energy the jet cross section is dominated by gg - and qg -initiated parton processes. Therefore, there is a chance that the measurement of the polarized jet cross section at RHIC will be useful in order to rule out some of the polarized sets that are at present consistent with the data. However, since we see from fig. 6 that the

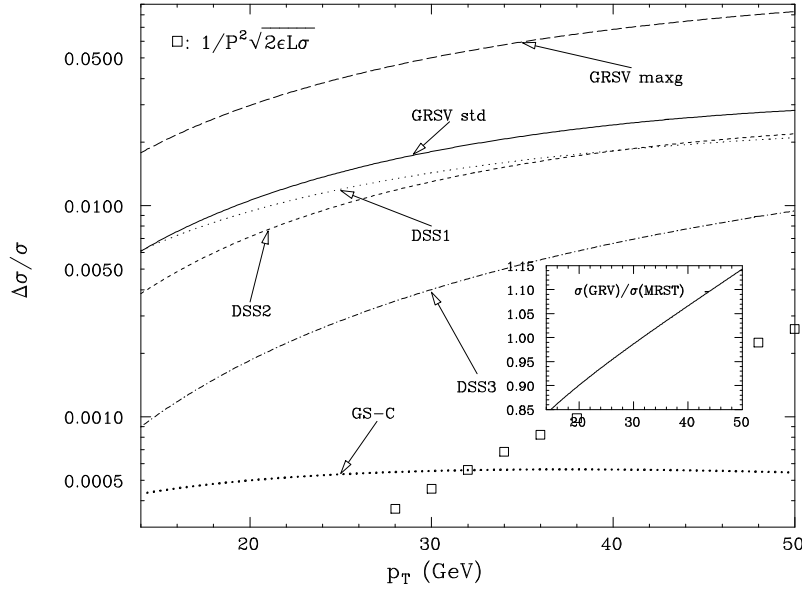


Figure 6: *Asymmetry versus transverse momentum for various polarized parton densities. The minimum measurable value for the asymmetry is also shown.*

asymmetry is always rather small, regardless of the specific densities used, the statistics will have to be large. To estimate the minimum value of the asymmetry observable at RHIC, we use the well-known formula

$$(\mathcal{A}_{p_T})_{min} = \frac{1}{P^2} \frac{1}{\sqrt{2\sigma\mathcal{L}\epsilon}}, \quad (5.2)$$

where \mathcal{L} is the integrated luminosity, P is the polarization of the beam, and the factor $\epsilon \leq 1$ accounts for experimental efficiencies; σ is the unpolarized cross section integrated over a small range in transverse momentum (p_T bin). The quantity defined in eq. (5.2) is plotted (boxes) in fig. 6, for $\epsilon = 1$, $P = 0.7$, $\mathcal{L} = 100 \text{ pb}^{-1}$ and a p_T -bin size of 2 GeV. From the figure we see that the asymmetry defined in eq. (5.1) is measurable if the polarized parton densities are as described by most of the sets considered here. On the other hand, if the densities are as suggested by the GS-C set, the measurement will be possible only by combining a large statistics with a good overall efficiency (clearly, it is also possible to enlarge the bin size, in this way decreasing the minimum observable asymmetry, at the price of losing resolution). As a general feature, we may notice that the slope of the minimum observable asymmetry is steeper than the slope of the theoretically predicted asymmetries, increasing with increasing transverse momentum. This means that, although the value of the asymmetry is larger at high p_T than at small p_T , the measurement in this region will be more problematic. We also point out that, apart from the case of GS-C, the shape of the asymmetries obtained with the different parton density sets is rather similar, which just reflects the fact that the various gluon densities are rather similar in shape.

We can still argue that the values for the asymmetry displayed in fig. 6 are artificially small, because of the different values of Λ_{QCD} used when computing $\Delta\sigma$ and σ . In the latter

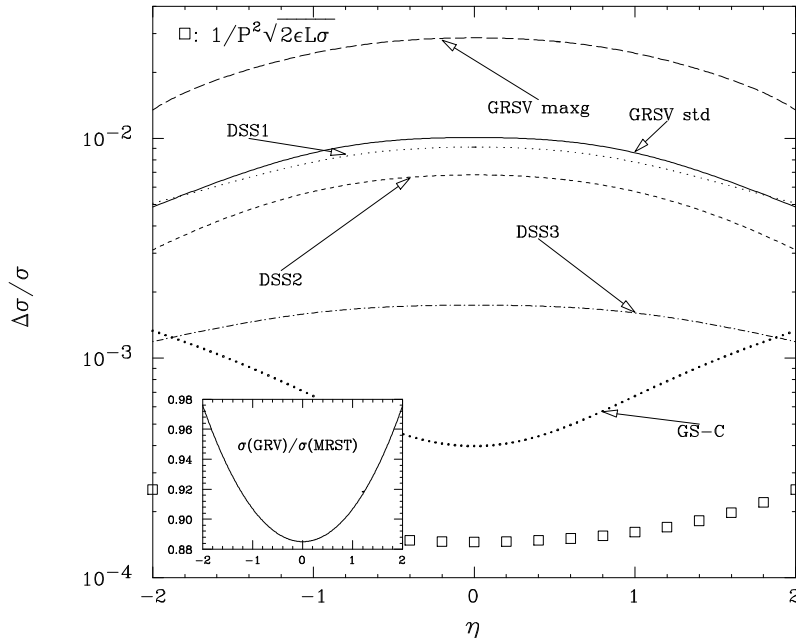


Figure 7: *Asymmetry versus pseudo-rapidity for various polarized parton densities. The minimum measurable value for the asymmetry is also shown.*

case, the MRST set has $\Lambda_5^{\overline{\text{MS}}} = 220$ MeV, while in the former case the typical value is around $\Lambda_5^{\overline{\text{MS}}} = 130$ MeV. For this reason, in the inset of fig. 6 we plot the ratio of the unpolarized cross sections obtained with the MRST and the GRV sets (the GRV set has $\Lambda_5^{\overline{\text{MS}}} = 131$ MeV). We see that if we had plotted the asymmetries using GRV instead of MRST, the final result would differ by 15% at the most, with respect to what is shown in fig. 6. Our previous conclusions are therefore unaffected by the choice of the unpolarized densities. Finally, we verified that, if one defines the jets using a cone algorithm instead of the ES algorithm, the results are practically unchanged: as one might have anticipated, the details of the jet definition ‘cancel’ in the ratio that defines the asymmetry.

The definition given in eq. (5.1) can be generalized to any single-inclusive or double-differential observable. In fig. 7 we plot the asymmetry for single-inclusive jet production, as a function of the pseudo-rapidity of the jet, with a cut $p_T > 15$ GeV. As should be clear from the small- p_T region of fig. 6, also in this case all the predictions obtained with different density sets lie above the minimum observable asymmetry calculated with $\epsilon = 1$ and $\mathcal{L} = 100$ pb $^{-1}$ (the bin size is 0.2). As in the case of transverse momentum, all the shapes are rather similar, except for the one relevant to GS-C, which has a local minimum at $\eta = 0$. The study of the asymmetry in the region around $\eta = 0$ could therefore be used to infer information on the shape of the polarized gluon density. We verified again that fig. 7 is unchanged if we use a jet-finding algorithm based upon a cone prescription.

We also computed single-inclusive asymmetries at the Born level. The results differ from those presented in fig. 6 and fig. 7 for a factor up to 20%. The shape is also different. Therefore, NLO corrections give non-trivial information on the structure of the asymmetries.

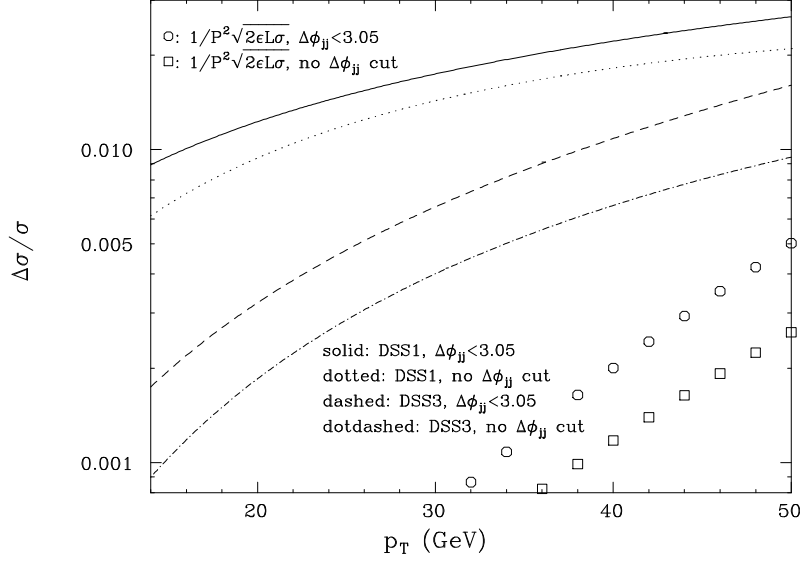


Figure 8: *Asymmetry versus transverse momentum. The effect of a cut on the azimuthal distance between the two leading jets of the event is shown.*

The possibility remains that, in some regions of the phase space, the asymmetry is larger than that shown in figs. 6 and 7, and therefore that the measurement of the polarized cross section turns out to be easier. In the following we give a simple example. By inspection of our results for double-differential observables, we noticed that the $\Delta\phi_{jj}$ correlation is steeper in the case of unpolarized collisions than in the case of polarized ones. In other words, the fraction of events with $\Delta\phi_{jj} \simeq \pi$ is higher in unpolarized collisions with respect to polarized collisions. This means that, by rejecting all the events with $\Delta\phi_{jj} \simeq \pi$, the asymmetry will be enhanced. We therefore considered all the events with at least two jets, and we evaluated the azimuthal distance $\Delta\phi_{jj}$ between the two leading jets. We eventually rejected all the events with $\Delta\phi_{jj} > 3.05$. For all the jets in the events passing this cut, we then computed the asymmetry as given in eq. (5.1). The results are shown in fig. 8, for two different parton density sets, superimposed on the results already shown in fig. 6 obtained with the same parton densities. As we expected, the value of the asymmetry is indeed increased, by a factor of about 1.5 to 2. However, if we compute the minimum observable asymmetry as indicated before, we see that this quantity also increased (since the unpolarized cross section has decreased by effect of the $\Delta\phi_{jj}$ cut). It follows that the measurement of the asymmetry in the case of a $\Delta\phi_{jj}$ cut will be as difficult as in the case when no cut is applied (and, in the high- p_T region, even more difficult). On the other hand, such a possibility is still interesting in the sense that it can be used as a valuable test of the predictions of perturbative QCD, since the observable shown in fig. 8 is more exclusive than the one presented in fig. 6.

We finally consider some double differential observables, namely $\Delta\phi_{jj}$, M_{jj} , $\Delta\eta_{jj}$ and the x_1 -distribution, defined in the previous section; the results are presented in terms of $\Delta\sigma$ in fig. 9. For the plots shown in that figure we choose the cuts as given in eqs. (4.2) and (4.4). Each observable is computed with the six different parton density sets used previously in

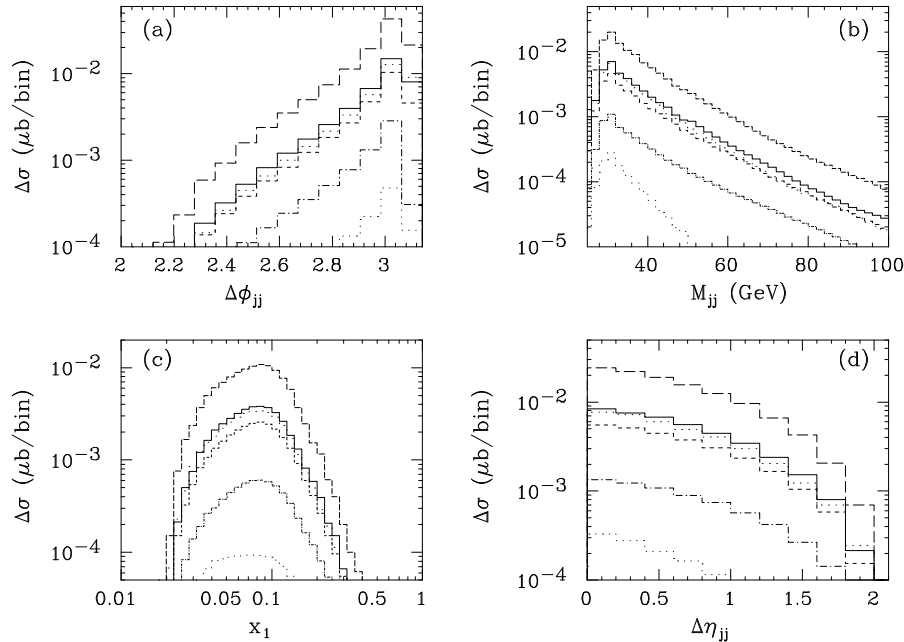


Figure 9: *Double differential observables in polarized collisions for various parton densities. The order of the cross sections is the same as in fig 7.*

the case of asymmetries. We see that, for $\Delta\phi_{jj}$, x_1 and η_{jj} , the shape of the distributions is rather insensitive to the choice of the densities. A somewhat more pronounced dependence is displayed in the case of the invariant mass M_{jj} . In fact, the typical value for the Bjorken x probed in two-jet events is of the order of M_{jj}/\sqrt{S} . We explicitly verified that the pattern shown in fig. 9 is not modified if we define the jets with a cone algorithm. The same is also true if we change the scales from their default values, except for the $\Delta\phi_{jj} \simeq \pi$ region, where the scale dependence is very large and the shape of the distribution is sizeably modified. This is due to the well-known fact that this region is particularly sensitive to the emission of quasi-soft gluons, and a resummation to all orders would be needed to get a reliable theoretical prediction. As discussed in section 4 we do not have a similar problem in the small- M_{jj} region, because of the asymmetric cuts in the transverse momenta of the two leading jets.

6 Conclusions

In this paper, we have presented the first complete calculation at next-to-leading order in perturbative QCD of one-jet and two-jet cross sections in polarized hadronic collisions. To this end, we extended the general formalism of ref. [12], based upon the subtraction method and relevant for unpolarized incoming beams, to the case of polarized beams. The resulting formulae together with the matrix elements of refs. [9, 10] can be easily implemented in a Monte Carlo code. We used the code presented in ref. [14] for unpolarized hadron-hadron

collisions, and we suitably modified it in order to deal with the polarized case⁵. The program outputs the momenta of the final-state partons plus a weight. The momenta are eventually used in an analysis routine to define the physical observables. During the same computer run, we can obtain predictions for an arbitrary number of one-jet and two-jet quantities, using several jet-finding algorithms, as well as predictions for other infrared-safe observables, such as shape variables. We stress that, in spite of these features, the code is not equivalent to a Monte Carlo parton shower generator, being the result of a fixed-order perturbative QCD calculation.

Using the aforementioned code, we investigated in some detail the phenomenological implications of jet production at RHIC (polarized pp collisions with a maximum centre-of-mass energy of 500 GeV). We first studied the scale dependence of single-inclusive and double-differential jet observables, in order to determine whether the next-to-leading order results are reliable enough to give sensible theoretical predictions. We found that the next-to-leading order corrections sizeably reduce the scale dependence with respect to the Born results. Furthermore, the polarized next-to-leading order cross sections display a scale dependence comparable to that of the corresponding unpolarized cross sections. We then turned to the study of the dependence of our results upon the choice of the polarized parton densities. These quantities are very poorly constrained by the available DIS data at present, especially for the gluon density, which enters the dominant contributions to the jet cross sections in the RHIC energy range. It follows that, depending upon the specific parton density set adopted, our predictions can vary by about two orders of magnitude. This fact in turn implies that measurements of jet observables at RHIC will be helpful in constraining the polarized densities. In fact, we have shown that, if the design integrated luminosity will be obtained, a detailed study of the polarized jet cross sections will be possible.

Acknowledgements

We warmly acknowledge J.Ph. Guillet for his collaboration at an early stage of this work. The work of D.deF. was partially supported by the World Laboratory (project T1). This work was supported in part by the EU Fourth Framework Programme ‘Training and Mobility of Researchers’, Network ‘Quantum Chromodynamics and the Deep Structure of Elementary Particles’, contract FMRX-CT98-0194 (DG 12-MIHT).

Appendix: Parton Generator for Polarized Hadron–Hadron Scattering

We will briefly describe here the main differences between parton generators for unpolarized and polarized hadron–hadron scattering. A detailed description of the method can be found in ref. [14]; here we only explicitly present the steps necessary to convert the parton generator of ref. [14] into a parton generator relevant to polarized collisions.

⁵The codes for both the polarized and unpolarized collisions are available upon request.

As already mentioned, a fake measurement function is used to disentangle the various infrared singularities appearing in the phase space, in order to apply the subtraction method to terms that contain one soft and one collinear singularity at most. In this respect, there is no difference between the cases of polarized and unpolarized scattering. Furthermore, the proof of ref. [12], that the singularities which appear in the intermediate steps of the calculation eventually cancel in the sum that defines physically observable quantities, also goes unchanged. This is due to the fact that, as in the unpolarized case, the singular part of a matrix element has the form of a reduced matrix element convoluted with a universal (i.e. process-independent) kernel.

We start from eq. (2.1); as in ref. [14], we will deal in the following with the case of $N - 1$ jet production. We write the polarized partonic cross section at NLO as

$$d\hat{\sigma}_{a_1 a_2}(\lambda_1; \lambda_2) = d\hat{\sigma}_{a_1 a_2}^{(0)}(\lambda_1; \lambda_2) + d\hat{\sigma}_{a_1 a_2}^{(1,N)}(\lambda_1; \lambda_2) + d\hat{\sigma}_{a_1 a_2}^{(1,N-1)}(\lambda_1; \lambda_2), \quad (\text{A.1})$$

where $d\hat{\sigma}_{a_1 a_2}^{(0)}$ is the Born contribution. All the terms in the RHS of eq. (A.1) are *finite*; $d\hat{\sigma}_{a_1 a_2}^{(1,N)}$ ($d\hat{\sigma}_{a_1 a_2}^{(1,N-1)}$) corresponds to configurations with N ($N - 1$) partons in the final state.

The N -parton contribution reads (see eq. (A.1) of ref. [14])

$$d\hat{\sigma}_{a_1 a_2}^{(1,N)}(\lambda_1; \lambda_2) = \sum_{i=3}^{N+2} \left(d\sigma_{a_1 a_2, i}^{(in,f)}(\lambda_1; \lambda_2) + \sum_{\substack{j=3 \\ j \neq i}}^{N+2} d\sigma_{a_1 a_2, ij}^{(out,f)}(\lambda_1; \lambda_2) \right). \quad (\text{A.2})$$

The quantities $d\sigma_{a_1 a_2, i}^{(in,f)}(\lambda_1; \lambda_2)$ and $d\sigma_{a_1 a_2, ij}^{(out,f)}(\lambda_1; \lambda_2)$ can be obtained from eqs. (A.3) and (A.11) of ref. [14] respectively, with the formal substitution of the matrix elements squared with their polarized counterpart

$$\mathcal{M}^{(N)}(\{a_l\}_1^{N+2}) \longrightarrow \mathcal{M}^{(N)}(\{a_l\}_1^{N+2}; \lambda_1; \lambda_2). \quad (\text{A.3})$$

Notice that in the unpolarized case the quantity $\mathcal{M}^{(N)}$ also includes an average factor for the sum over the polarizations of the incoming partons, which must be removed in the present case.

The $(N - 1)$ -parton contribution reads (see eq. (A.15) of ref. [14])

$$d\hat{\sigma}_{a_1 a_2}^{(1,N-1)}(\lambda_1; \lambda_2) = d\hat{\sigma}_{a_1 a_2}^{(1,N-1v)}(\lambda_1; \lambda_2) + d\hat{\sigma}_{a_1 a_2}^{(1,N-1r)}(\lambda_1; \lambda_2). \quad (\text{A.4})$$

The quantity $d\hat{\sigma}_{a_1 a_2}^{(1,N-1v)}(\lambda_1; \lambda_2)$ can be obtained from eqs. (A.16), (A.23), (A.24) and (A.25) of ref. [14], with formal substitutions analogous to that of eq. (A.3)

$$\mathcal{M}^{(N-1)}(\{a_l\}_1^{N+1}) \longrightarrow \mathcal{M}^{(N-1)}(\{a_l\}_1^{N+1}; \lambda_1; \lambda_2), \quad (\text{A.5})$$

$$\mathcal{M}_{ij}^{(N-1)}(\{a_l\}_1^{N+1}) \longrightarrow \mathcal{M}_{ij}^{(N-1)}(\{a_l\}_1^{N+1}; \lambda_1; \lambda_2), \quad (\text{A.6})$$

$$\mathcal{M}_{NS}^{(N-1,v)}(\{a_l\}_1^{N+1}) \longrightarrow \mathcal{M}_{NS}^{(N-1,v)}(\{a_l\}_1^{N+1}; \lambda_1; \lambda_2). \quad (\text{A.7})$$

We stress the fact that the coefficients $\mathcal{Q}(\{a_l\}_1^{N+1})$ and $\mathcal{I}_{ij}^{(reg)}$, which appear in eq. (A.16) of ref. [14], are not modified in the polarized case. The reason is the following: \mathcal{Q} gets

contributions from the final-state collinear configurations, which are summed over polarizations, and from the soft part ($z = 1$) of the Altarelli–Parisi kernels relevant to initial-state collinear configurations, which is the same in the polarized and unpolarized cases. $\mathcal{I}_{ij}^{(reg)}$ is obtained by integration of the eikonal factors, which appear in the soft limit of the N -parton matrix element squared in both the polarized and unpolarized cases. The information on the polarizations of the incoming partons is therefore fully contained in Born matrix elements squared (eq. (A.5)), in the colour-linked Born matrix elements squared (eq. (A.6)), and in the finite part of the virtual contribution (eq. (A.7)). The colour-linked matrix elements can be defined exactly as in ref. [20], using Born amplitudes summed only over the helicities of the final-state partons.

The quantity $d\hat{\sigma}_{a_1 a_2}^{(1, N-1r)}(\lambda_1; \lambda_2)$ in the polarized case is only slightly more complicated than in the unpolarized case, eq. (A.26) of ref. [14]. We get

$$\begin{aligned}
d\hat{\sigma}_{a_1 a_2}^{(1, N-1r)}(K_1, \lambda_1; K_2, \lambda_2) &= \frac{\alpha_S}{4\pi} \sum_d \int d\xi \mathcal{O}_{da_1}(\xi) d\Xi_1 \sigma_{da_2}^{(0)}((1-\xi)K_1; K_2, \lambda_2) \\
&+ \frac{\lambda_1}{|\lambda_1|} \frac{\alpha_S}{4\pi} \sum_d \int d\xi \Delta \mathcal{O}_{da_1}(\xi) d\Delta_1 \sigma_{da_2}^{(0)}((1-\xi)K_1; K_2, \lambda_2) \\
&+ \frac{\alpha_S}{4\pi} \sum_d \int d\xi \mathcal{O}_{da_2}(\xi) d\Xi_2 \sigma_{a_1 d}^{(0)}(K_1, \lambda_1; (1-\xi)K_2) \\
&+ \frac{\lambda_2}{|\lambda_2|} \frac{\alpha_S}{4\pi} \sum_d \int d\xi \Delta \mathcal{O}_{da_2}(\xi) d\Delta_2 \sigma_{a_1 d}^{(0)}(K_1, \lambda_1; (1-\xi)K_2),
\end{aligned} \tag{A.8}$$

where

$$d \begin{pmatrix} \Xi_1 \\ \Delta_1 \end{pmatrix} \sigma_{ab}(\lambda) = d\sigma_{ab}(+; \lambda) \pm d\sigma_{ab}(-; \lambda), \tag{A.9}$$

$$d \begin{pmatrix} \Xi_2 \\ \Delta_2 \end{pmatrix} \sigma_{ab}(\lambda) = d\sigma_{ab}(\lambda; +) \pm d\sigma_{ab}(\lambda; -). \tag{A.10}$$

The form of the operator \mathcal{O}_{ab} can be read from eq. (A.26) of ref. [14]:

$$\begin{aligned}
\mathcal{O}_{ab}(\xi) &= \xi P_{ab}^{<}(1-\xi, 0) \left[\left(\frac{1}{\xi} \right)_c \log \frac{S\delta_I}{2\mu^2} + 2 \left(\frac{\log \xi}{\xi} \right)_c \right] \\
&- \xi P_{ab}'^{<}(1-\xi, 0) \left(\frac{1}{\xi} \right)_c - K_{ab}(1-\xi),
\end{aligned} \tag{A.11}$$

where $P_{ab}^{<}(z, 0) + \epsilon P_{ab}'^{<}(z, 0) + \mathcal{O}(\epsilon^2)$ are the unpolarized Altarelli–Parisi kernels for $z < 1$ in $4 - 2\epsilon$ dimensions, and K_{ab} define the scheme for the unpolarized parton densities (in the $\overline{\text{MS}}$ scheme they are equal to zero). We also have

$$\begin{aligned}
\Delta \mathcal{O}_{ab}(\xi) &= \xi \Delta P_{ab}^{<}(1-\xi, 0) \left[\left(\frac{1}{\xi} \right)_c \log \frac{S\delta_I}{2\mu^2} + 2 \left(\frac{\log \xi}{\xi} \right)_c \right] \\
&- \xi \Delta P_{ab}'^{<}(1-\xi, 0) \left(\frac{1}{\xi} \right)_c - \Delta K_{ab}(1-\xi),
\end{aligned} \tag{A.12}$$

where, as usual,

$$\Delta P_{ab}^< = P_{a+b+}^< - P_{a-b+}^<. \quad (\text{A.13})$$

It is now trivial to get the quantities $d\Delta\hat{\sigma}_{a_1a_2}$ which appear in eq. (2.3). From eqs. (A.1), (A.2) and (A.4) we get

$$\begin{aligned} d\Delta\hat{\sigma}_{a_1a_2} &= d\Delta\hat{\sigma}_{a_1a_2}^{(0)} + \sum_{i=3}^{N+2} \left(d\Delta\sigma_{a_1a_2,i}^{(in,f)} + \sum_{\substack{j=3 \\ j \neq i}}^{N+2} d\Delta\sigma_{a_1a_2,ij}^{(out,f)} \right) \\ &+ d\Delta\hat{\sigma}_{a_1a_2}^{(1,N-1v)} + d\Delta\hat{\sigma}_{a_1a_2}^{(1,N-1r)}. \end{aligned} \quad (\text{A.14})$$

The first four terms in the RHS of this equation can be obtained from the corresponding terms in the unpolarized case with the substitution

$$\mathcal{M} \longrightarrow \Delta\mathcal{M}, \quad (\text{A.15})$$

which directly follows from eqs. (A.3), (A.5)–(A.7). The form for $d\Delta\hat{\sigma}_{a_1a_2}^{(1,N-1r)}$ can be directly obtained from eq. (A.8). We have

$$\begin{aligned} d\Delta\hat{\sigma}_{a_1a_2}^{(1,N-1r)}(K_1; K_2) &= \frac{\alpha_s}{2\pi} \sum_d \int d\xi \Delta\mathcal{O}_{da_1}(\xi) d\Delta\sigma_{da_2}^{(0)}((1-\xi)K_1; K_2) \\ &+ \frac{\alpha_s}{2\pi} \sum_d \int d\xi \Delta\mathcal{O}_{da_2}(\xi) d\Delta\sigma_{a_1d}^{(0)}(K_1; (1-\xi)K_2), \end{aligned} \quad (\text{A.16})$$

which is in fact completely analogous to eq. (A.26) of ref. [14].

In summary, the main structure of a computer code which evaluates jet cross sections is identical in the unpolarized and polarized cases. No conceptual modification is required; in particular, there is no need to deal explicitly with the polarizations of the incoming hadrons/partons. The full information on the polarizations can be embedded in the ‘polarized’ Altarelli–Parisi kernels ΔP , and in the ‘polarized’ matrix elements $\Delta\mathcal{M}$. Both quantities can be treated as black boxes, exactly like the corresponding quantities in the unpolarized case.

References

- [1] For a compilation of references to the data, see P.J. Mulders and T. Sloan, Summary talk of Spin Physics Working Group at the 6th International Workshop on Deep Inelastic Scattering and QCD, Brussels (1998), hep-ph/9806314.
- [2] M. Glück, E. Reya, M. Stratmann and W. Vogelsang, *Phys. Rev.* **D53** (1996) 4775.
- [3] T. Gehrmann and W.J. Stirling, *Phys. Rev.* **D53** (1996) 6100.
- [4] D. de Florian, O.A. Sampayo and R. Sassot, *Phys. Rev.* **D57** (1998) 5803.

- [5] C. Bourrely *et al.*, hep-ph/9803229;
L. Gordon, M. Goshtasbpour and G.P. Ramsey, hep-ph/9803351;
E. Leader, A.V. Sidorov and D.B. Stamenov, hep-ph/9807251.
- [6] M. Stratmann, in proceedings of the ‘2nd Topical Workshop on Deep Inelastic Scattering off Polarized Targets: Theory Meets Experiment (SPIN 97)’, DESY-Zeuthen, Germany, September 1997, p. 94., hep-ph/9710379.
- [7] R.D. Ball, S. Forte and G. Ridolfi, *Phys. Lett.* **B378** (1996) 255;
G. Altarelli, R.D. Ball, S. Forte and G. Ridolfi, *Nucl. Phys.* **B496** (1997) 337;
G. Altarelli, R.D. Ball, S. Forte and G. Ridolfi, Talks given at Cracow Epiphany Conference on Spin Effects in Particle Physics and Tempus Workshop, Cracow, Poland, 9-11 Jan 1998. *Acta Phys.Polon.* **B29** (1998) 1145, hep-ph/9803237.
- [8] J. Soffer and J.M. Virrey, *Nucl. Phys.* **B509** (1998) 297.
- [9] Z. Bern and D.A. Kosower, *Nucl. Phys.* **B379** (1992) 451;
Z. Kunszt, A. Signer and Z. Trócsányi, *Nucl. Phys.* **B411** (1994) 397.
- [10] R. Gastmans and T.T. Wu, *The Ubiquitous Photon*, 1990, Clarendon Press, Oxford.
- [11] W.T. Giele and E.W.N. Glover, *Phys. Rev.* **D46** (1992) 1980;
W.T. Giele, E.W.N. Glover and D.A. Kosower, *Nucl. Phys.* **B403** (1993) 633.
- [12] S. Frixione, Z. Kunszt and A. Signer, *Nucl. Phys.* **B467** (1996) 399.
- [13] S. Catani and M. Seymour, *Nucl. Phys.* **B485** (1997) 291 (Erratum *Nucl. Phys.* **B510** (1998) 503).
- [14] S. Frixione, *Nucl. Phys.* **B507** (1997) 295.
- [15] J.C. Collins, D.E. Soper and G. Sterman, in *Perturbative Quantum Chromodynamics*, ed. A. Mueller, 1989, World Scientific, Singapore, and references therein.
- [16] S. Ellis and D.E. Soper, *Phys. Rev.* **D48** (1993) 3160.
- [17] M. Glück, E. Reya and A. Vogt, *Z. Phys.* **C67** (1995) 433.
- [18] A.D. Martin, R.G. Roberts, W.J. Stirling and R.S. Thorne, *Eur. Phys. J.* **C4** (1998) 463.
- [19] S. Frixione and G. Ridolfi, *Nucl. Phys.* **B507** (1997) 315.
- [20] Z. Kunszt and D.E. Soper, *Phys. Rev.* **D46** (1992) 192.